RSC Advances

PAPER

View Article Online
View Journal | View Issue

Cite this: *RSC Adv.*, 2015, **5**, 67979

Luminescence and energy transfer of co-doped $Sr_5MgLa_2(BO_3)_6:Ce^{3+},Mn^{2+}$

Matthias Müller, Stefan Fischer and Thomas Jüstel*

In this work the photoluminescence (PL) of co-doped $Sr_5MgLa_2(BO_3)_6:Ce^{3+},Mn^{2+}$ as well as the energy transfer (ET) from Ce^{3+} to Mn^{2+} was examined. To this end, powder samples with different Mn^{2+} concentrations were synthesised *via* high temperature solid state reaction. Phase purity of prepared samples was investigated by X-ray powder diffraction. To elucidate the PL properties of $Sr_5MgLa_2(BO_3)_6:Ce^{3+},Mn^{2+}$, emission and excitation spectra along with diffuse reflectance spectra were recorded. Additionally, fluorescence lifetime measurements were performed. To study the temperature behaviour of the emission of $Sr_5MgLa_2(BO_3)_6:Ce^{3+},Mn^{2+}$, PL and lifetime measurements were conducted from 100 to 500 K. Furthermore, external quantum efficiencies were determined and chromaticity coordinates were calculated. It was found that co-doped $Sr_5MgLa_2(BO_3)_6:Ce^{3+},Mn^{2+}$ possesses two emission bands located in the violet/blue and deep red range of the electromagnetic spectrum. Moreover, it turned out that ET from Ce^{3+} to Mn^{2+} in $Sr_5MgLa_2(BO_3)_6:Ce^{3+},Mn^{2+}$ takes place *via* an exchange interaction mechanism. Temperature dependent PLD measurements reveal that thermal quenching of emission is mainly caused by the Mn^{2+} ions. Finally, quantum efficiency of Ce^{3+} doped $Sr_5MgLa_2(BO_3)_6:Ce^{3+}$ was found to be close to unity.

Received 3rd July 2015
Accepted 28th July 2015

DOI: 10.1039/c5ra12951f

www.rsc.org/advances

1. Introduction

In the last two decades light emitting diodes (LEDs) have more and more replaced conventional light sources like incandescent or fluorescent lamps. This is due to the benefits LEDs provide to lighting installations over traditional light sources. Commonly, LEDs provide longer lifetime, higher wall plug efficiency, as well as a higher colour rendering.[1] Nowadays most of the white emitting LEDs consist of a blue emitting (In,Ga)N-chip combined with a green-yellow emitting phosphor, *e.g.* $Y_3Al_5O_{12}:Ce^{3+}$.[2] These light sources provide high luminous efficiency due to intense emission in the green spectral range. On the other site, due to the lack of red emission these systems suffer from a high colour temperature and low colour rendering index (CRI) which is unintended for domestic lighting.[3] On that account an alternative approach to generate warm white light with appropriate CRI is the combination of a blue, green, and red phosphor excited by an ultraviolet (UV) emitting LED. In this way LEDs with excellent colour temperature as well as convenient CRI can be designed.[4] Unfortunately, these packages incur a loss in blue emission due to reabsorption by the green and red phosphors. This is why many groups try to develop single phase white emitting phosphors which convert UV radiation into white light.[5] One strategy to realize such a phosphor is to use the ion couple Ce^{3+} and Mn^{2+}.[6] In many host materials Ce^{3+} and Mn^{2+} possess broad emission bands in the blue and red spectral range, respectively.[7] Due to additive colour mixing these emission bands can complement each other to white light. Further, the broad excitation band of the spin and parity allowed $[Xe]4f^1$–$[Xe]5d^1$ transition in Ce^{3+} is suitable for pumping with UV LEDs. Since all transitions in Mn^{2+} are fully forbidden, the blue emission of Ce^{3+} can also be used for sensitizing the $[Ar]3d^5$–$[Ar]3d^5$ excitation transition *via* energy transfer (ET).

To investigate the photoluminescence (PL) properties as well as the ET from Ce^{3+} to Mn^{2+} in co-activated $Sr_5MgLa_2(BO_3)_6:Ce^{3+},Mn^{2+}$ a series of powder samples with various Mn^{2+} contents was prepared. $Sr_5MgLa_2(BO_3)_6$ belongs to a class of *ortho*-borates, firstly described by Schaffers *et al.* in 1994.[8] Further, Sankar and Rao reported on the PL of different compositions of said material with numerous activators.[9,10] $Sr_5MgLa_2(BO_3)_6$ crystalizes in a high-symmetry trigonal structure with space group $R\bar{3}$. $Sr_5MgLa_2(BO_3)_6$ comprises a 9-fold coordinated site as well as two different octahedrally coordinated sites. The 9-fold coordinated sites are shared by Sr^{2+} and La^{3+} ions in the ratio 0.67 to 0.33. The octahedrally coordinated sites differ in average bond length of the surrounding oxygen ions. The larger sites exhibit an average bond length of 0.2298 Å and are occupied by Sr^{2+} ions whereas the smaller octahedral sites with a mean distance of 0.2092 Å are occupied by Mg^{2+} ions. The ionic radii of La^{3+} and Sr^{2+} for 9-fold coordination are 1.216 and 1.13 Å. Sr^{2+} and Mg^{2+} exhibit ionic radii of 1.18 and 0.72 Å in an octahedral coordination. The ionic radii of Ce^{3+} for 9-fold and 6-fold coordination are 1.01 and 1.196 Å. 6-fold coordinated Mn^{2+} has

Department of Chemical Engineering, Münster University of Applied Sciences, Stegerwaldstrasse 39, 48565 Steinfurt, Germany. E-mail: tj@fh-muenster.de

an ionic radius of 0.83 Å.[11] Considering the ionic radii as well as charge balancing, it is assumed that the Ce^{3+} ions primarily going to occupy the 9-fold coordinated La^{3+} sites whereas Mn^{2+} ions tend to occupy the octahedral Mg^{2+} sites.

In this contribution, synthesis, optical properties, and ET from Ce^{3+} to Mn^{2+} in co-doped $Sr_5MgLa_2(BO_3)_6$:Ce^{3+},Mn^{2+} are discussed. Therefore, samples with different doping concentrations were prepared *via* high temperature solid state synthesis. Phase purity was validated using X-ray powder diffractometry (XRD). Diffuse reflectance (DR) spectra were recorded to examine the body colour of $Sr_5MgLa_2(BO_3)_6$:Ce^{3+},Mn^{2+}. PL properties were investigated by recording PL spectra and photoluminescence excitation spectra (PLE). Temperature behaviour of the PL was examined by recording PL spectra from 100 to 500 K. In addition, photoluminescence decay (PLD) measurements were performed from 100 to 500 K to study the origin of thermal quenching. To monitor the ET from Ce^{3+} to Mn^{2+} PLD measurements were performed on samples with different Mn^{2+} concentrations. Furthermore, external quantum efficiencies η_{ext} were determined and chromaticity coordinates according to Commission International de l'Eclairage 1931 (CIE) were calculated.

2. Experimental

All investigated $Sr_5MgLa_2(BO_3)_6$:Ce^{3+},Mn^{2+} samples were prepared by high temperature solid state synthesis. To this end, high purity educts $SrCO_3$ (Aldrich, 99.9%), MgO (Merck KGaA, p.a.), La_2O_3 (Treibacher Industrie AG, 99.995%), H_3BO_3 (Merck KGaA, Ph. Eur.), CeO_2 (Atomergic Chemetals Co., 99.9%), and $MnC_2O_4 \cdot 2H_2O$ (Dr Paul Lohmann, chem. pure) were weighted in stoichiometric amounts. Though, an excess of 5% of boric acid was used to compensate evaporation. The starting materials were thoroughly blended in acetone in an agate mortar. After drying at ambient temperatures, the obtained powder blends were heated at 650 °C for 1 h in air to decompose the boric acid. Afterwards, the samples were ground and calcined at 1200 °C for 6 h in a corundum crucible imbedded in active carbon. Obtained white sinter bodies were subsequently ground to a fine μ-powder.

Phase purity of the synthesized $Sr_5MgLa_2(BO_3)_6$:Ce^{3+},Mn^{2+} samples was investigated using XRD. XRD patterns were collected on a Rigaku MiniFlex II diffractometer working in Bragg–Brentano geometry using Cu K_α radiation. Step width and integration time were set to 0.02° and 1 s, respectively.

PL spectra as well as PLE spectra were recorded on an Edinburgh Instruments FSL900 spectrometer equipped with a Xe arc lamp (450 W) and a cooled (−20 °C) single-photon counting photomultiplier (Hamamatsu R2658P). Obtained PL spectra were corrected by applying a correction file obtained from a tungsten incandescent lamp certified by the National Physics Laboratory U.K.

For PLD measurements on Ce^{3+}, a picosecond pulsed LED (40 μW, pulse width = 912.6 ps, λ_{em} = 267 nm) was attached to the spectrometer. For PLD measurements on Mn^{2+} a microsecond pulsed Xe lamp (100 W, pulse width = 1 μs) was used.

PL measurements at 2.9 K were performed using the closed cycle cryocooler OptistatAC-V12 from Oxford Instruments. Helium was used as a cooling agent. Temperature dependent PL measurements from 100 to 500 K were performed using the Oxford Instruments cryostat MicrostatN2. Liquid nitrogen was used as a cooling agent. Temperature stabilization time was 60 s and tolerance was set to ±3 K.

DR spectra were recorded on an Edinburgh Instruments FS900 spectrometer equipped with a Xe arc lamp (450 W), a cooled (−20 °C) single-photon counting photomultiplier (Hamamatsu R928) as well as a Teflon-coated integration sphere. $BaSO_4$ (99.998%, Sigma-Aldrich) was used as a reflectance standard.

External quantum efficiencies η_{ext} were determined using the approach of Kawamura *et al.*[12] Therefore, PL spectra of the samples as well as of the excitation source were recorded in a Teflon-coated integration sphere. From this, η_{ext} can be calculated using the following relation:

$$\eta_{ext} = \frac{\int I_{em}(\lambda)d\lambda}{\int I_{ex}(\lambda)d\lambda - \int I'_{ex}(\lambda)d\lambda} \quad (1)$$

here, $I_{em}(\lambda)$ is the emission intensity of the sample, $I_{ex}(\lambda)$ is the intensity of the excitation lamp in absence of the sample and $I'_{ex}(\lambda)$ is the intensity of the excitation lamp in presence of the sample.

3. Results and discussion

To investigate phase purity of the synthesised $Sr_5MgLa_2(BO_3)_6$ samples XRD patterns were recorded. Fig. 1 shows the collected XRD patterns of doped and undoped $Sr_5MgLa_2(BO_3)_6$ as well as the ICDD reference card of $Sr_5MgLa_2(BO_3)_6$. The diffractograms indicate the formation of the trigonal $Sr_5MgLa_2(BO_3)_6$ phase. No change in the host structure can be observed with increasing doping concentration. This observation confirms the suitability of the utilized synthesis route.

Fig. 2 depicts the DR spectra of undoped $Sr_5MgLa_2(BO_3)_6$ as well as of $Sr_5Mg(La_{0.99}Ce_{0.01})_2(BO_3)_6$ and $Sr_5Mg_{0.97}Mn_{0.03}La_2(BO_3)_6$. The undoped $Sr_5MgLa_2(BO_3)_6$ sample shows an absorption band in the UV range below 400 nm. This band is tentatively assigned to band-to-band absorption of the host structure.[9] The absorption in the DR spectrum of $Sr_5Mg(La_{0.99}Ce_{0.01})_2(BO_3)_6$ is assigned to the spin and parity allowed $[Xe]4f^1$–$[Xe]5d^1$ interconfigurational electric-dipole transition in Ce^{3+}. The DR spectrum of $Sr_5Mg_{0.97}Mn_{0.03}La_2(BO_3)_6$ shows slight absorption at about 470 nm which is ascribed to the transition from the $^6A_1(^6S)$ ground state to the $^4T_1(^4G)$ excited state in Mn^{2+}.

Room temperature PLE and PL spectra of singly doped $Sr_5Mg(La_{0.99}Ce_{0.01})_2(BO_3)_6$ and $Sr_5Mg_{0.97}Mn_{0.03}La_2(BO_3)_6$ as well as of co-doped $Sr_5Mg_{0.90}Mn_{0.10}(La_{0.99}Ce_{0.01})_2(BO_3)_6$ are depicted in Fig. 3a–c. The PLE spectrum of $Sr_5Mg(La_{0.99}Ce_{0.01})_2(BO_3)_6$ (Fig. 3a) was recorded monitoring the 400 nm-emission and shows a broad band ranging from about 240 to 370 nm. This band consists of various unresolved bands due to excitation

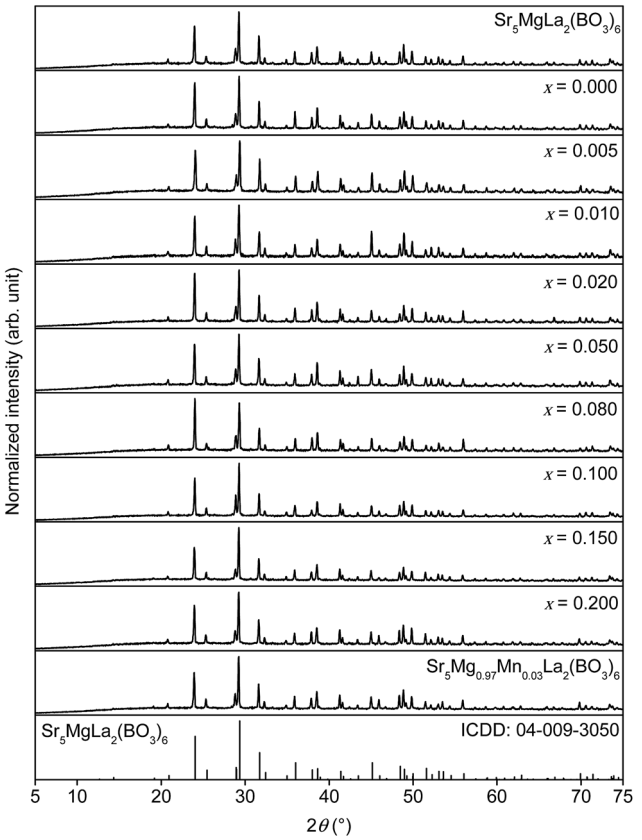

Fig. 1 XRD patterns of $Sr_5MgLa_2(BO_3)_6$, $Sr_5Mg_{1-x}Mn_x(La_{0.99}Ce_{0.01})_2(BO_3)_6$, $Sr_5Mg_{0.97}Mn_{0.03}La_2(BO_3)_6$, and ICDD reference card.

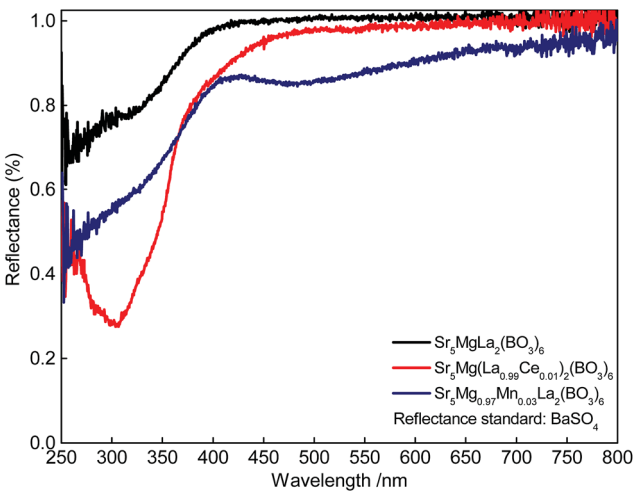

Fig. 2 DR spectra of $Sr_5MgLa_2(BO_3)_6$, $Sr_5Mg(La_{0.99}Ce_{0.01})_2(BO_3)_6$, and $Sr_5Mg_{0.97}Mn_{0.03}La_2(BO_3)_6$.

from the $^2F_{7/2,5/2}$ ground state to the [Xe]$5d^1$ multiplet of Ce^{3+}. The PL spectrum of $Sr_5Mg(La_{0.99}Ce_{0.01})_2(BO_3)_6$ was recorded using an excitation wavelength of $\lambda_{ex} = 300$ nm. The spectrum exhibits a broad band peaking at about 397 nm and a tailing towards lower energy of the electromagnetic range. This emission band occurs due to radiative relaxation from the excited ^2D_j state of the [Xe]$5d^1$ configuration to the $^2F_{7/2,5/2}$ ground state of Ce^{3+}. The tailing is caused by Ce^{3+} ions occupying different lattice sites and will be discussed later in the article in more detail. Fig. 3b illustrates the PLE and PL spectra of $Sr_5Mg_{0.97}Mn_{0.03}La_2(BO_3)_6$. Monitoring the 715 nm-emission of Mn^{2+}, the obtained PLE spectrum exhibits various bands at about 305, 319, 354, 378, 398, 415 and 474 nm. These bands were attributed to transitions from the $^6A_1(^6S)$ ground state to $^4T_1(^4F)$, $^4A_2(^4F)$, $^4T_1(^4P)$, $^4E(^4D)$, $^4T_2(^4D)$, $[^4E(^4G)^4A_1(^4G)]$, and $^4T_1(^4G)$, respectively. The PL spectrum of $Sr_5Mg_{0.97}Mn_{0.03}La_2(BO_3)_6$ shows a broad band with a maximum at about 714 nm and a tailing to the long wavelength range. This emission is due radiative relaxation from the $^4T_1(^4G)$ excited state to the $^6A_1(^6S)$ ground state in Mn^{2+}. PLE and PL spectra of $Sr_5Mg_{0.90}Mn_{0.10}(La_{0.99}Ce_{0.01})_2(BO_3)_6$ are depicted in Fig. 3c. PLE spectra were recorded monitoring the emission of Mn^{2+} and Ce^{3+} at 715 and 400 nm, respectively. The obtained PLE spectra appear similar in shape indicating the occurrence of ET from Ce^{3+} ions to Mn^{2+} ions. The PL spectrum was recorded upon excitation with a wavelength of $\lambda_{ex} = 300$ nm and shows two bands peaking at about 403 and 713 nm. These bands originate from radiative relaxation from [Xe]$5d^1$ to $^2F_{7/2,5/2}$ in Ce^{3+} and from $^4T_1(^4G)$ to $^6A_1(^6S)$ in Mn^{2+}.

For further investigations on the origin of the tailing of the Ce^{3+} emission band, a PL spectrum of $Sr_5Mg(La_{0.99}Ce_{0.01})_2(BO_3)_6$ was recorded at 2.9 K. This spectrum is illustrated in Fig. 4. Commonly, Ce^{3+} emission consists of a doublet band due to spin–orbit-splitting of the ^2F state ([Xe]$4f^1$ configuration) into the $^2F_{7/2}$ and $^2F_{5/2}$ states. The energetic difference between the $^2F_{7/2}$ and $^2F_{5/2}$ states usually amounts to about 2000 cm^{-1}.[13]

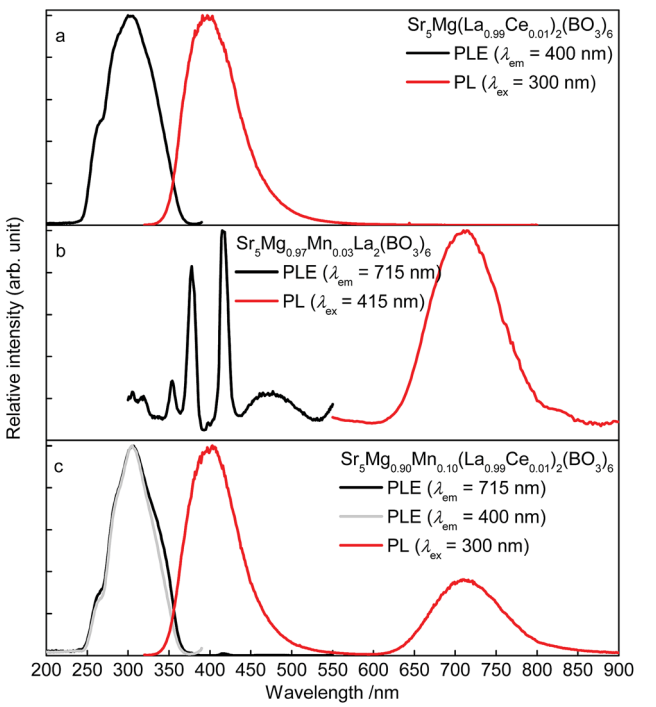

Fig. 3 Room temperature PLE and PL spectra of $Sr_5Mg(La_{0.99}Ce_{0.01})_2(BO_3)_6$ (a), $Sr_5Mg_{0.97}Mn_{0.03}La_2(BO_3)_6$ (b), $Sr_5Mg_{0.90}Mn_{0.10}(La_{0.99}Ce_{0.01})_2(BO_3)_6$ (c).

Therefore, it should be possible to fit the present Ce^{3+} emission band with two Gaussian curves with an approximate distance of 2000 cm^{-1}. However, fitting the current PL spectrum with two Gaussian curves leads to an approximate distance of about 1399 cm^{-1}. This indicates the occupation of more than one distinct crystallographic site. This is thoroughly possible since $Sr_5MgLa_2(BO_3)_6$ provides also 6-fold coordinated Sr^{2+} sites aside from the 9-fold coordinated site. Against this, fitting the Ce^{3+} emission band with a sum of four Gaussian curves A, B, C, and D results in approximate distances of 2018 and 1979 cm^{-1}. Based on this result, it is assumed that the Ce^{3+} ions also occupy the 6-fold coordinated Sr^{2+} sites. Since crystal field splitting of the 5d states decreases with increasing coordination number, the energetic difference between d and f states increases. Therefore, it is concluded that curves A and B belong to Ce^{3+} occupying a 6-fold coordinated Sr^{2+} site (Ce2) whereas curves C and D were assigned to Ce^{3+} on a 9-fold coordinated site (Ce1). The occupation of two different crystallographic sites is also reflected in the PLE spectra depicted in the inset of Fig. 4. Monitoring the emission of Ce^{3+} at 345, 380, and 415 nm results in PLE spectra looking significantly different in shape. Shifting the monitored wavelength from 345 to 415 nm, the obtained PLE spectrum gets broader and a new band arises. This observation also indicates PL from different crystallographic sites.

Fig. 5 depicts PL spectra of $Sr_5Mg_{1-x}Mn_x(La_{0.99}Ce_{0.01})_2(BO_3)_6$ with $x = 0.000$, 0.005, 0.010, 0.020, 0.050, 0.080, 0.100, 0.150, and 0.200. Up to a Mn^{2+} content of $x = 0.100$ PL intensity of Mn^{2+} increases. At higher Mn^{2+} contents, the PL intensity of Mn^{2+} starts to decrease due to concentration quenching. Furthermore, with increasing Mn^{2+} content the Ce^{3+} PL intensity decreases implying the occurrence of ET from Ce^{3+} to Mn^{2+}.

Further, fluorescence lifetime measurements were performed monitoring the Ce^{3+} emission of co-doped $Sr_5Mg_{1-x}Mn_x(La_{0.99}Ce_{0.01})_2(BO_3)_6$. The obtained PLD curves are plotted in Fig. 6 and can be best fitted with a bi-exponential function using the following equation:

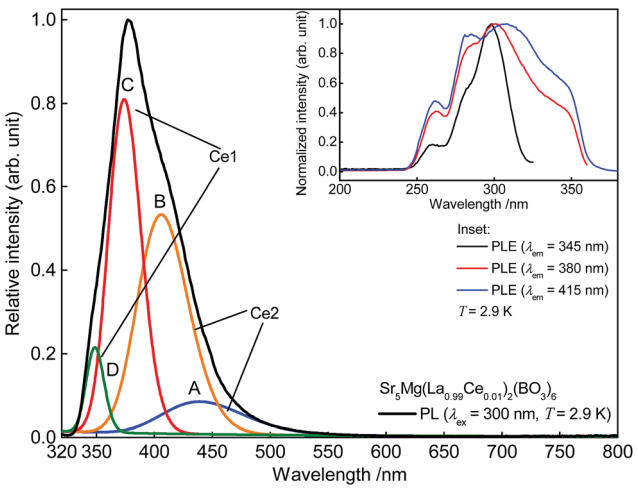

Fig. 4 Low temperature PL spectra of $Sr_5Mg(La_{0.99}Ce_{0.01})_2(BO_3)_6$ and Gaussian curves A, B, C, and D. Inset: low temperature PLE spectra of $Sr_5Mg(La_{0.99}Ce_{0.01})_2(BO_3)_6$.

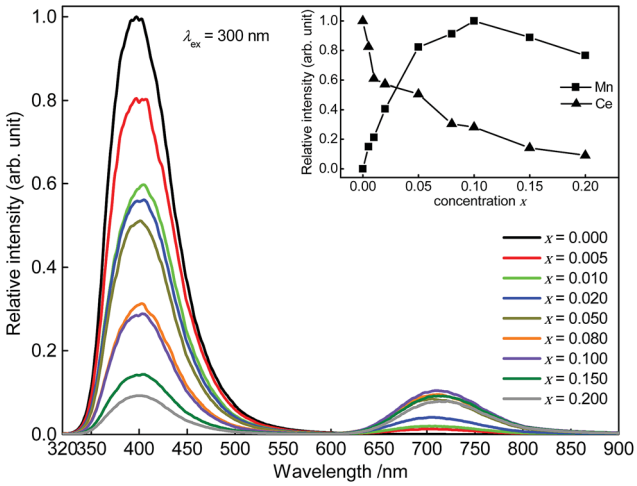

Fig. 5 PL spectra of $Sr_5Mg_{1-x}Mn_x(La_{0.99}Ce_{0.01})_2(BO_3)_6$. Inset: integrated PL intensity in dependence of the Ce^{3+} and Mn^{2+} concentration.

$$I(t) = A_1 e^{\frac{-t}{\tau_1}} + A_2 e^{\frac{-t}{\tau_2}} \quad (2)$$

here, I is the PL intensity at the time t, A_1 and A_2 are fitting parameters, and τ_1 and τ_2 are the partial fluorescence lifetimes of the exponential components. The bi-exponential behaviour of the PLD curves reflects PL of two different crystallographic sites as detailed above. The average fluorescence lifetimes τ of the Ce^{3+} emission were obtained applying eqn (3):

$$\tau = \frac{A_1\tau_1^2 + A_2\tau_2^2}{A_1\tau_1 + A_2\tau_2} \quad (3)$$

Calculated average fluorescence lifetimes τ as well as the emission fractions $frac_1$ and $frac_2$ are summarized in Table 1. It turned out that with increasing Mn^{2+} content fluorescence lifetimes τ of the Ce^{3+} emission decreases. Since ET processes are magnitudes faster than radiative transitions, this behaviour indicates the occurrence of ET from Ce^{3+} to Mn^{2+}. The ET efficiency η_T can be calculated using the following equation:[14]

$$\eta_T = 1 - \frac{\tau_S}{\tau_{S0}} \quad (4)$$

here, τ_S and τ_{S0} are the fluorescence lifetimes of Ce^{3+} in presence and absence of Mn^{2+}. The calculated values for η_T are summarized in Table 1 and also plotted in the inset of Fig. 6. It can be seen that the values for η_T show a continuous growth with increasing Mn^{2+} content.

To identify the nature of the ET from Ce^{3+} to Mn^{2+} in co-doped $Sr_5La_2Mg(BO_3)_6$:Ce^{3+},Mn^{2+} Dexter's approach of exchange interactions and multipolar interactions was used.

On the basis of Dexter's ET formula and Reisfeld's approximation the following relations are obtained:[15]

$$\ln\left(\frac{\eta_0}{\eta}\right) \propto C \quad (5)$$

$$\frac{\eta_0}{\eta} \propto C^{\frac{\alpha}{3}} \quad (6)$$

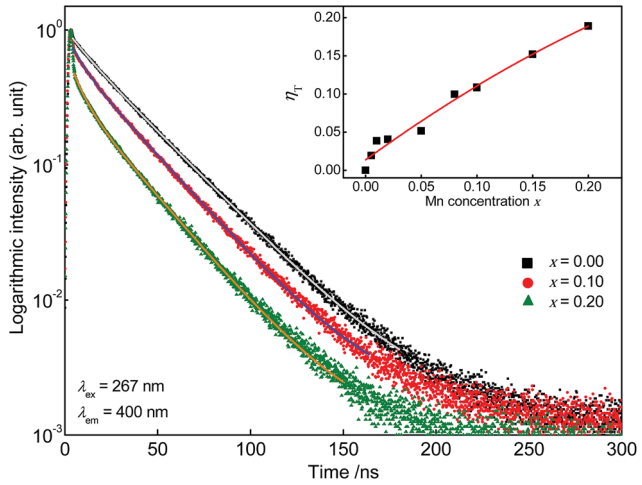

Fig. 6 PLD curves of $Sr_5Mg_{1-x}Mn_x(La_{0.99}Ce_{0.01})_2(BO_3)_6$. Inset: ET transfer efficiency η_T in dependence of the Mn^{2+} concentration.

Table 1 Fluorescence lifetimes τ as well as partial lifetimes τ_1 and τ_2 and the emission fractions $frac_1$ and $frac_2$ of Ce^{3+} and ET efficiency η_T in $Sr_5Mg_{1-x}Mn_x(La_{0.99}Ce_{0.01})_2(BO_3)_6$

Sample (x)	$frac_1$ (%)	τ_1 (ns)	$frac_2$ (%)	τ_2 (ns)	τ (ns)	η_T
0.000	4	9.3	96	31.0	30	0
0.005	5	9.4	95	30.7	30	0.02
0.010	5	8.9	95	30.1	29	0.04
0.020	4	7.5	96	30.0	29	0.04
0.050	6	8.5	94	29.9	29	0.05
0.080	7	6.9	93	28.7	27	0.10
0.100	7	6.3	93	28.5	27	0.11
0.150	11	7.6	89	27.8	26	0.15
0.200	12	6.7	88	27.0	25	0.19

In these equations η_0 and η are the internal luminescence quantum efficiencies of Ce^{3+} in the absence and presence of Mn^{2+}. C is the concentration of Mn^{2+} in the samples. Eqn (5) corresponds to exchange interaction whereas eqn (6) with $\alpha = 6$, 8, and 10 corresponds to dipole–dipole, dipole–quadrupole, and quadrupole–quadrupole interaction, respectively. η_0 and η can approximately be estimated by the fluorescence lifetimes τ_0 and τ. Fig. 7 shows the plots of relation (5) and (6). A linear behaviour is only observed for relation (5) and suggests ET *via* exchange interaction.

To validate this result, the integrated PL intensities of the Ce^{3+} and Mn^{2+} emission were investigated using van Uitert's approach:[16]

$$\frac{I}{I_0} = \left(1 + Ax^{\frac{\theta}{3}}\right)^{-1} \quad (7)$$

here, I and I_0 are the luminescence Intensities in the absence and presence of Mn^{2+}, A is a constant, and x is the concentration of Mn^{2+} ions. $\theta = 3$, 6, 8, and 10 represents exchange interaction, dipole–dipole, dipole–quadrupole, and quadrupole–quadrupole interactions, respectively.[17] Experimental data is plotted in Fig. 8 and best fitting is obtained when plugging in 3 for θ. This also suggests that ET from Ce^{3+} to Mn^{2+} in $Sr_5MgLa_2(BO_3)_6$:Ce^{3+},Mn^{2+} occurs *via* exchange interaction. This observation is rather uncommon for the ET from Ce^{3+} and Mn^{2+}. Since exchange interactions proceed only over short distances this result implies a non-statistical distribution of the Ce^{3+} and Mn^{2+} ions. To estimate the critical distance between Ce^{3+} and Mn^{2+} further investigations were carried out using the Inokuti–Hirayama equation for exchange interaction:[18]

$$\frac{I(t)}{I_0} = \exp\left[-\left(\frac{t}{\tau}\right) - \left(\frac{C}{C_0}\right)\gamma^{-3}g(z)\right] \quad (8)$$

In this equation $I(t)$ is the intensity at a certain time and I_0 is the intensity after excitation. t is the time and τ is the intrinsic fluorescence lifetime of Ce^{3+} in absence of Mn^{2+}. C is the concentration of Mn^{2+} ions per unit volume and C_0 is the critical concentration. γ is the transfer volume and $g(z)$ is defined as

$$g(z) = -z\int_0^1 \exp(-zy)(\ln y)^3 \mathrm{d}y \quad (9)$$

here, z and y are defined as

$$z = \exp\left(\gamma\frac{t}{\tau}\right) \quad (10)$$

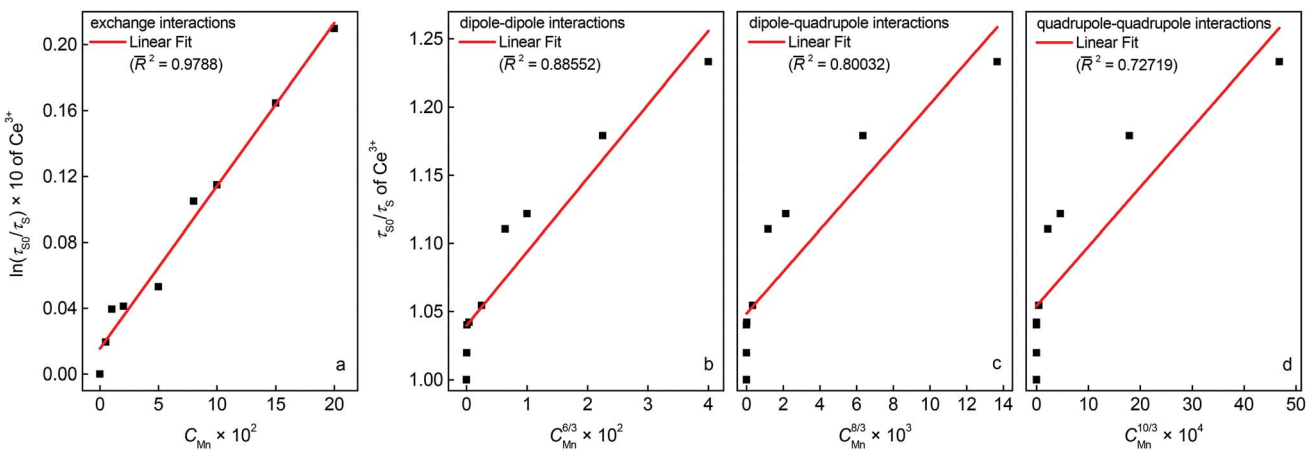

Fig. 7 Dependence of $\ln(\tau_0/\tau)$ on C_{Mn} (a) and τ_0/τ on $C^{6/3}$ (b), $C^{8/3}$ (c), and $C^{10/3}$ (d).

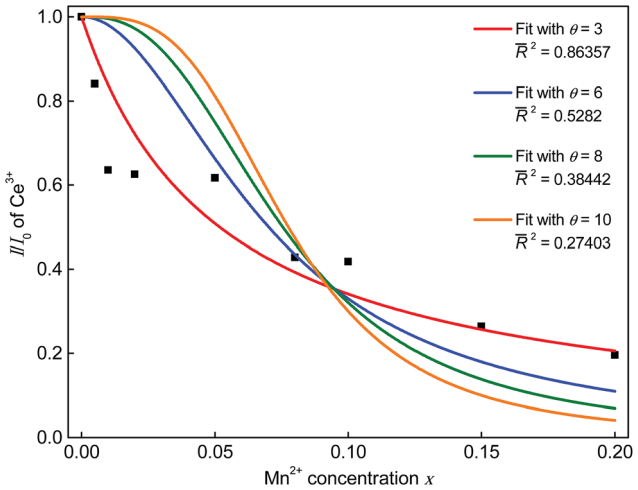

Fig. 8 Dependence of I/I_0 on the Mn^{2+} concentration.

$$y = \exp\left(-\gamma \frac{R}{R_0}\right) \tag{11}$$

Eqn (9) can be expressed by a Taylor series as described by Inokuti and Hirayama which converges. This leads to the following formula:

$$\frac{I(t)}{I_0} = \exp\left[-\left(\frac{t}{\tau}\right) - \left(\frac{C}{C_0}\right)\gamma^{-3} \times \left((\ln z)^3 + h_1(\ln z)^2 + h_2(\ln z) + h_3\right)\right] \tag{12}$$

For the coefficients h_1, h_2, and h_3 the values 1.73164699, 5.93433597, and 5.44487446, respectively, given by Inokuti and Hirayama were plugged in. Fitting the PLD curves of the investigated samples with eqn (12) yields the C/C_0 values. C/C_0 values are plotted against $3/(4\pi R_c^3)$ in Fig. 9. Since $C_0 = 3/(4\pi R_c^3)$, the slope of a linear fit through the data points is equal to R_c^3.[18,19] Therefore, the critical distance R_c for ET from Ce^{3+} to Mn^{2+} was calculated to be 4.6 Å.

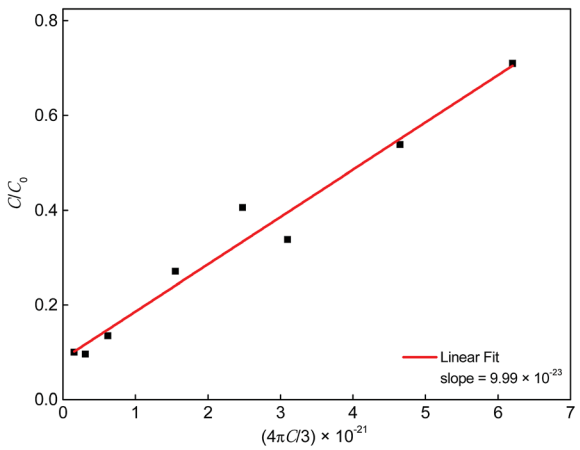

Fig. 9 Dependence of C/C_0 on $4\pi C/3$.

To investigate the temperature behaviour of the PL of $Sr_5Mg_{0.90}Mn_{0.10}(La_{0.99}Ce_{0.01})_2(BO_3)_6$ PL spectra from 100 to 500 K were recorded. The obtained PL spectra are illustrated in Fig. 10. Due to thermal quenching, the PL intensity of Ce^{3+} and Mn^{2+} decreases with increasing temperature. In addition, the maximum of the Mn^{2+} emission band shows a shift towards higher energy of the electromagnetic spectrum. Since the equilibrium distance between the Mn^{2+} ions and its oxygen ligands extends with increasing temperature, the energy difference of the $^4T_1(^4G) \rightarrow {}^6A_1(^6S)$ transition increases.[20] Therefore, the maximum of the Mn^{2+} emission is shifted towards the blue range. The inset of Fig. 10 depicts the PL integrals of the Ce^{3+} and Mn^{2+} emission bands in dependence of temperature. By fitting the data points with a Fermi–Dirac distribution activation energy E_A for thermal quenching can be calculated.

$$I(T) = \frac{I_0}{1 + B \times e^{\frac{-E_A}{kT}}} \tag{13}$$

here, $I(T)$ is the integrated PL intensity at a certain temperature and I_0 is the PL intensity at zero Kelvin. B is the frequency factor for thermal quenching, T is the temperature and k is the Boltzmann constant ($k = 8.617 \times 10^{-5}$ eV K^{-1}). The values of the parameters I_0 and B were derived from the fitting function and are about 0.95 and 333, respectively. Fitting the data points with this equation yields an activation energy of $E_A = 0.18$ eV. From this the $T_{1/2}$ value can be derived by using the following relation:

$$T_{1/2} = \frac{-E_A}{k \times \ln\left(\frac{1}{B}\right)} \tag{14}$$

$T_{1/2}$ describes the temperature at which PL intensity of a luminescent centre is decreased to one-half of its maximum intensity. For the investigated $Sr_5Mg_{0.90}Mn_{0.10}(La_{0.99}Ce_{0.01})_2(BO_3)_6$ sample $T_{1/2}$ was calculated to be 355 K.

For further investigations on the origin of thermal quenching in $Sr_5Mg_{0.90}Mn_{0.10}(La_{0.99}Ce_{0.01})_2(BO_3)_6$ fluorescence lifetime

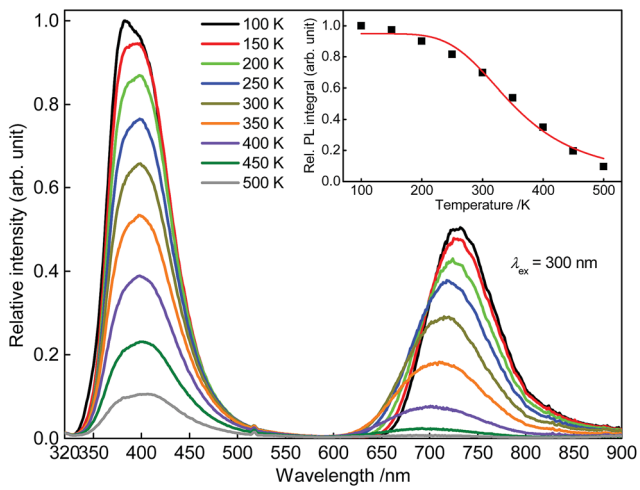

Fig. 10 PL spectra of $Sr_5Mg_{0.90}Mn_{0.10}(La_{0.99}Ce_{0.01})_2(BO_3)_6$ from 100 to 500. Inset: integrated PL intensity in dependence of temperature.

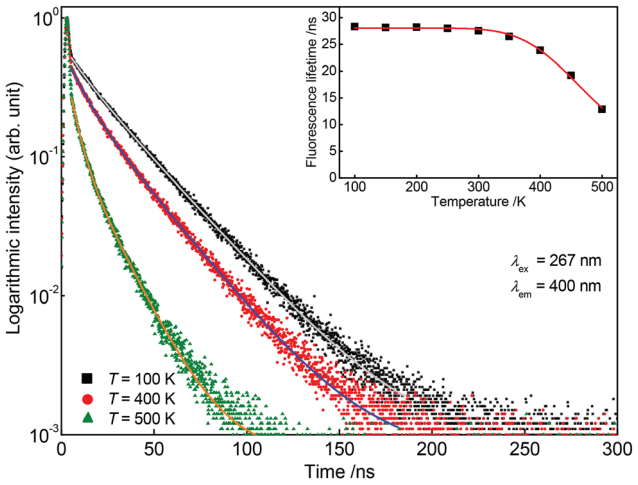

Fig. 11 Obtained PLD curves of $Sr_5Mg_{0.90}Mn_{0.10}(La_{0.99}Ce_{0.01})_2(BO_3)_6$ at 100, 400, and 500 K monitoring the PL of Ce^{3+}. Inset: Fluorescence lifetimes of the Ce^{3+} emission in dependence of temperature.

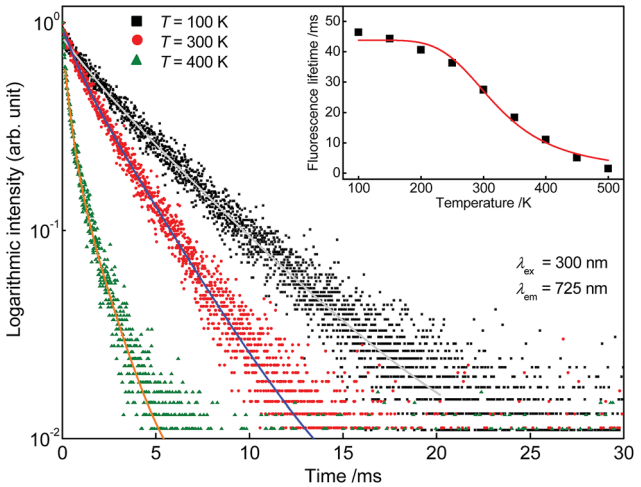

Fig. 12 Obtained PLD curves of $Sr_5Mg_{0.90}Mn_{0.10}(La_{0.99}Ce_{0.01})_2(BO_3)_6$ at 100, 300, and 400 K monitoring the PL of Mn^{2+}. Inset: Fluorescence lifetimes of the Mn^{2+} emission in dependence of temperature.

measurements were performed. Therefore, PLD curves of the Ce^{3+} as well as of the Mn^{2+} emission were recorded from 100 to 500 K. Fig. 11 depicts the obtained PLD curves monitoring the 400 nm-emission of Ce^{3+}. The PLD curves show a bi-exponential behaviour reflecting PL from two distinct crystallographic sites as mentioned above. The fluorescence lifetimes of Ce^{3+} are illustrated in the inset of Fig. 11 and are summarized in Table 2. From this finding it can be derived that the fluorescence lifetimes remain stable up to a temperature of 300 K. At 350 K the fluorescence lifetimes start to decrease indicating a decline of radiative transitions due to thermal quenching. Fig. 12 shows the PLD curves of Mn^{2+} monitoring the emission at 725 nm. It is obvious from the inset that the Mn^{2+} PL lifetimes decrease continuously over the complete temperature range. Fitting the fluorescence lifetimes of Ce^{3+} and Mn^{2+} with eqn (13) yields the $T_{1/2}$ values for the Ce^{3+} ($T_{1/2,Ce}$) and Mn^{2+} ($T_{1/2,Mn}$) emission. $T_{1/2,Ce}$ and $T_{1/2,Mn}$ were calculated to be 492 and 323 K, respectively. This result indicates that the overall thermal quenching of the PL in $Sr_5Mg_{0.90}Mn_{0.10}(La_{0.99}Ce_{0.01})_2(BO_3)_6$ is mainly caused by the presence of Mn^{2+}.

The efficiency of the prepared $Sr_5MgLa_2(BO_3)_6$:Ce^{3+},Mn^{2+} samples was examined by determining external quantum efficiency η_{ext} as mentioned above. To our understanding, η_{ext} is defined as the ratio between the number of emitted photons $N_{emission}$ and the number of absorbed photons $N_{absorption}$:

$$\eta_{ext} = \frac{N_{emission}}{N_{absorption}} \quad (15)$$

The calculated external quantum efficiencies are summarized in Table 3. It turned out that with increasing Mn^{2+} concentration η_{ext} continuously decreases. This is probably caused by concentration quenching due to ET between the Mn^{2+} ions.

To illustrate the colour of the emission, CIE chromaticity coordinates were calculated according to the relevant PL spectra. The obtained colour points are depicted in Fig. 13. All colour points are located in the violet region of the chromaticity coordinates diagram. With increasing Mn^{2+} content the colour points show a shift towards the red region. Since the Mn^{2+}

Table 2 Fluorescence lifetimes τ as well as partial lifetimes τ_1 and τ_2 and the emission fractions $frac_1$ and $frac_2$ of Ce^{3+} and Mn^{2+} in $Sr_5Mg_{1-x}Mn_x(La_{0.99}Ce_{0.01})_2(BO_3)_6$ from 100 to 500 K

	Ce^{3+}					Mn^{2+}				
T (K)	τ_1 (ns)	$frac_1$ (%)	τ_2 (ns)	$frac_2$ (%)	τ (ns)	τ_1 (ms)	$frac_1$ (%)	τ_2 (ms)	$frac_2$ (%)	τ (ms)
100	10.6	8	29.7	92	28	14.8	6	48.2	94	46
150	9.6	7	29.6	93	28	13.1	5	45.9	95	44
200	10.2	9	30.0	91	28	16.5	9	42.9	91	41
250	8.7	7	29.5	93	28	16.8	13	37.9	87	35
300	8.7	8	29.2	92	28	7.8	8	28.9	92	27
350	8.9	11	28.5	89	26	5.8	15	20.7	85	18
400	9.1	17	26.8	83	24	3.5	27	13.8	73	11
450	7.2	21	22.4	79	19	1.7	30	6.5	70	5
500	4.8	29	16.2	71	13	0.3	12	1.7	88	2

Table 3 External quantum efficiencies η_{ext} and CIE colour coordinates of $Sr_5Mg_{1-x}Mn_x(La_{0.99}Ce_{0.01})_2(BO_3)_6$

Sample (x)	η_{ext}	CIE (x|y)
0.000	0.97	(0.160|0.046)
0.005	0.72	(0.160|0.046)
0.010	0.53	(0.161|0.046)
0.020	0.57	(0.164|0.048)
0.050	0.53	(0.169|0.050)
0.080	0.33	(0.175|0.052)
0.100	0.33	(0.178|0.052)
0.150	0.20	(0.188|0.059)
0.200	0.18	(0.194|0.062)

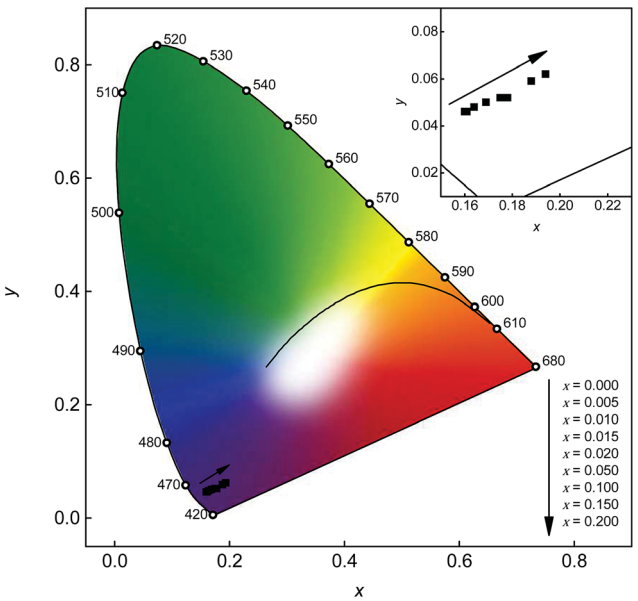

Fig. 13 CIE chromaticity diagram of $Sr_5Mg_{1-x}Mn_x(La_{0.99}Ce_{0.01})_2(BO_3)_6$ with different Mn^{2+} concentrations. Inset: Enlarged section of the relevant range.

emission band is located in the deep red range of the visible spectrum where the eye sensitivity is rather low, the observed shift of the colour points is rather low too. A larger shift into the red region of the chromaticity coordinates diagram using co-doped $Sr_5MgLa_2(BO_3)_6$:Ce^{3+},Mn^{2+} could be obtained using a lower Ce^{3+} content. In this way the Mn^{2+} emission would be more intense compared to the Ce^{3+} emission band resulting in a larger shift.

4. Conclusions

To investigate the PL properties and the ET between Ce^{3+} and Mn^{2+} of co-doped $Sr_5MgLa_2(BO_3)_6$:Ce^{3+},Mn^{2+} a series of powder samples with various Mn^{2+} contents was prepared. $Sr_5MgLa_2(BO_3)_6$:Ce^{3+},Mn^{2+} shows two emission bands located at 403 and 713 nm upon excitation at λ_{ex} = 300 nm. Low temperature PL measurement on the Ce^{3+} emission reveals that the Ce^{3+} ions mainly occupy the 9-fold coordinated sites as well as the 6-fold coordinated Sr^{2+} sites. This statement is backed by the bi-exponential PLD curves of $Sr_5Mg(La_{0.99}Ce_{0.01})_2(BO_3)_6$. The highest PL intensity was found for a Mn^{2+} content of $x = 0.100$. Furthermore, it was demonstrated that the ET from Ce^{3+} to Mn^{2+} occurs *via* an exchange interaction mechanism. Critical distance R_c was determined to be 4.6 Å. Temperature depended PL measurements prove a $T_{1/2}$ value of 355 K for $Sr_5Mg_{0.90}Mn_{0.10}(La_{0.99}Ce_{0.01})_2(BO_3)_6$. Furthermore, temperature dependent fluorescence lifetimes revealed that thermal quenching is mainly caused by the Mn^{2+} ions. Finally, the external quantum efficiencies η_{ext} were determined to be close to unity of the Ce^{3+} doped samples. With increasing Mn^{2+} η_{ext} continuously decreases. Calculated chromaticity coordinates are all located in the violet region of the CIE diagram. Therefore, co-doped $Sr_5MgLa_2(BO_3)_6$:Ce^{3+},Mn^{2+} with the herein investigated doping levels is not suitable as a white or red emitting phosphor.

Acknowledgements

The authors are grateful to Merck KGaA Darmstadt, Germany for generous financial support.

References

1 (*a*) C. Feldmann, T. Jüstel, C. R. Ronda and P. J. Schmidt, *Adv. Funct. Mater.*, 2003, **13**, 511–516; (*b*) E. F. Schubert and J. K. Kim, *Science*, 2005, **308**, 1274–1278.
2 S. Nakamura, P. Stephen and F. Gerhard, *The Blue Laser Diode: The Complete Story*, Springer-Verlag, Berlin/Heidelberg, 1997.
3 H. S. Jang, W. B. Im, D. C. Lee, D. Y. Jeon and S. S. Kim, *J. Lumin.*, 2007, **126**, 371–377.
4 Y. Uchida and T. Taguchi, *Opt. Eng.*, 2005, **44**, 124003.
5 M. Shang, C. Li and J. Lin, *Chem. Soc. Rev.*, 2014, **43**, 1372.
6 (*a*) M. Müller and T. Jüstel, *J. Lumin.*, 2014, **155**, 398–404; (*b*) T. Jia, Z. Ci, Q. Wu, G. Zhu, C. Wang and Y. Wang, *ECS J. Solid State Sci. Technol.*, 2015, **4**, R78–R82.
7 (*a*) R. Yu, H. Li, H. Ma, C. Wang, H. Wang and J. McKittrick, *J. Am. Ceram. Soc.*, 2014, **97**, 1151–1156; (*b*) Q. Liu, Y. Liu, Y. Ding, Z. Peng, Q. Yu, X. Tian and G. Dong, *J. Sol-Gel Sci. Technol.*, 2014, **71**, 276–282; (*c*) Y. Shi, Y. Wen, M. Que, G. Zhu and Y. Wang, *Dalton Trans.*, 2014, 2418–2423; (*d*) L. Wu, B. Wang, Y. Zhang, L. Li, H. R. Wang, H. Yi, Y. F. Kong and J. J. Xu, *Dalton Trans.*, 2014, 13845.
8 K. I. Schaffers, P. D. Thompson, T. Alekel III, J. R. Cox and D. A. Keszler, *Chem. Mater.*, 1994, **6**, 2014–2022.
9 R. Sankar and G. Subba Rao, *J. Alloys Compd.*, 1998, **281**, 126–136.
10 R. Sankar, *Solid State Sci.*, 2008, **10**, 1864–1874.
11 R. D. Shannon, *Acta Crystallogr., Sect. A: Cryst. Phys., Diffr., Theor. Gen. Crystallogr.*, 1976, **32**, 751–767.
12 Y. Kawamura, H. Sasabe and C. Adachi, *Jpn. J. Appl. Phys.*, 2004, **43**, 7729–7730.
13 (*a*) F. A. Kröger and J. Bakker, *Physica*, 1941, **8**, 628–646; (*b*) G. Blasse and A. Bril, *J. Chem. Phys.*, 1967, **47**, 5139–5145.
14 (*a*) H. C. Kandpal and H. B. Tripathi, *Indian J. Pure Appl. Phys.*, 1979, **17**, 587–589; (*b*) P. Paulose, G. Jose, V. Thomas, N. Unnikrishnan and M. Warrier, *J. Phys. Chem. Solids*, 2003, **64**, 841–846.

15 (*a*) D. L. Dexter, *J. Chem. Phys.*, 1953, **21**, 836; (*b*) D. L. Dexter and J. H. Schulman, *J. Chem. Phys.*, 1954, **22**, 1063; (*c*) R. Reisfeld, E. Greenberg, R. Velapoldi and B. Barnett, *J. Chem. Phys.*, 1972, **56**, 1698.
16 L. G. van Uitert, *J. Electrochem. Soc.*, 1967, **114**, 1048.
17 (*a*) L. Zhang, Z. Lu, P. Han, L. Wang and Q. Zhang, *J. Nanomater.*, 2012, **2012**, 1–7; (*b*) F. Zhang and W. Tang, *Luminescence*, 2015, **30**, 216–220.
18 M. Inokuti and F. Hirayama, *J. Chem. Phys.*, 1965, **43**, 1978.
19 J. S. Lee, S. Unithrattil and W. B. Im, *J. Alloys Compd.*, 2013, **555**, 297–303.
20 Y. Tanabe and S. Sugano, *J. Phys. Soc. Jpn.*, 1954, **9**, 766–779.